Applied Catalysis A: General 515 (2016) 170–178

Contents lists available at ScienceDirect

Applied Catalysis A: General

journal homepage: www.elsevier.com/locate/apcata

Hierarchical porous $ZnWO_4$ microspheres synthesized by ultrasonic spray pyrolysis: Characterization, mechanistic and photocatalytic NO_x removal studies

Yu Huang[a,b,*], Yunxia Gao[a], Qian Zhang[a], Jun-ji Cao[a,b], Ru-jin Huang[a,b], Wingkei Ho[c,**], Shun Cheng Lee[d]

[a] Key Lab of Aerosol Chemistry & Physics, Institute of Earth Environment, Chinese Academy of Sciences, Xi'an 710061, China
[b] State Key Lab of Loess and Quaternary Geology (SKLLQG), Institute of Earth Environment, Chinese Academy of Sciences, Xi'an 710061, China
[c] Department of Science and Environmental Studies, The Hong Kong Institute of Education, Hong Kong, China
[d] Department of Civil and Environmental Engineering, The Hong Kong Polytechnic University, Hung Hom, Hong Kong, China

ARTICLE INFO

Article history:
Received 19 September 2015
Received in revised form 29 January 2016
Accepted 5 February 2016
Available online 10 February 2016

Keywords:
Porous $ZnWO_4$ microsphere
NO_x degradation
Ultrasonic spray pyrolysis
Electron spin resonance spectroscopy (ESR)
Photocatalysis

ABSTRACT

Solar-light-driven photocatalysts with porous structure are preferred for gaseous pollutants removal at low concentration levels. In this study, hierarchical porous $ZnWO_4$ microspheres were synthesized by a facile ultrasonic spray pyrolysis method for the first time. The as-prepared $ZnWO_4$ samples were composed of microspheres with diameter ranging from 0.1 to 2 μm and it was revealed that these microspheres are formed by the self-assembly of nanoparticles. The photocatalytic performances of these microspheres were evaluated by the degradation of gaseous NO_x under simulated solar light irradiation. It was found that the $ZnWO_4$ batch synthesized at 700 °C exhibited superior photocatalytic activity to those synthesized at 650 °C and 750 °C as well as Degussa TiO_2 P25. Both $^{\bullet}OH$ and $O_2^{\bullet-}$ radicals were found to be the major reactive species involved for NO_x degradation as identified by electron spin resonance spectroscopy (ESR) method, which was consistent with the theoretical analysis. The excellent catalytic activity of ZWO-700 was attributed to its special hierarchical porous structure, which facilitated the separation/diffusion of the photogenerated charge carriers and the diffusion of intermediates and final products of NO_x oxidation. The photocatalytic NO_x removal mechanism over $ZnWO_4$ samples was also proposed. This study suggests that ultrasonic spray pyrolysis is a facile and scalable process to fabricate $ZnWO_4$ porous microspheres which are promising photocatalytic materials for gaseous pollutants purification.

1. Introduction

Nitrogen oxides (NO_x, the sum of NO and NO_2) are mainly emitted from combustion-related processes, and are one of the most important precursors for secondary organic aerosols (SOAs) formation which contribute 22–77% of the $PM_{2.5}$ mass concentrations in China during serious haze episode [1]. Therefore, it is essential to control and reduce NO_x concentrations to mitigate the air pollution problems in China. Various techniques have been developed for NO_x abatement, including selective catalytic and non-catalytic reduction [2,3], three-way catalysis [4], wet scrubbing and biofiltration [5,6], and adsorption [7]. However, most of these approaches have been hindered in application because they either need high temperature to initiate the catalytic conversion reactions or cause secondary pollution. Hence, novel and practical strategies for reducing atmospheric NO_x to levels that could improve the environment are urgently needed.

Photocatalysis is an effective and promising technique for environmental NO_x removal at ambient temperature, and it has attracted considerable attention in the past few decades [8]. $ZnWO_4$, with a wolframite structure, is one of the most important metal tungstates that has high potential applications in various fields as well as utilized for photocatalytic degradation of organic pollutants [9–13]. As it is well known, the crystallinity,

* Corresponding author at: Key Lab of Aerosol Chemistry & Physics, Institute of Earth Environment, Chinese Academy of Sciences, Xi'an 710061, China.
** Corresponding author at: Department of Science and Environmental Studies, The Hong Kong Institute of Education, Hong Kong, China.
E-mail addresses: huangyu@ieecas.cn (Y. Huang), keithho@ied.edu.hk (W. Ho).

http://dx.doi.org/10.1016/j.apcata.2016.02.007
0926-860X/

dimensions and morphology of photocatalysts are crucial to improve their catalytic performance [14,15]. Therefore, to enhance the photocatalytic activity of $ZnWO_4$, various methodologies including conventional solid-state reactions, microwave-assisted precipitation, and hydro/solvothermal methods have been adopted to prepare $ZnWO_4$ photocatalysts with different microstructures and tunable properties [10,11,14,16–20]. For example, $ZnWO_4$ nanoparticles and nanorods were successfully synthesized via kinetic and thermodynamic control processes by hydrothermal method, and it was demonstrated that the perfect crystallinity of $ZnWO_4$ nanorods can enhance the photocatalytic activity [10]. $ZnWO_4$ with cubic morphology [16], nanocrystals [21], yolk-shell microspheres [20], nanorods with different aspect ratio [22] were also synthesized for photocatalysis application in recent years. The effects of morphology on the photocatalytic activity of $ZnWO_4$ are also discussed in several studies. Photocatalysts with porous structures could possess high surface areas to facilitate the mass transfer of reactants, which is crucial for the efficient elimination of gaseous pollutants at low concentration levels [23]. However, there was no reported study about porous structured $ZnWO_4$ fabrication and application in photocatalysis for air purification.

Ultrasonic spray pyrolysis (USP) method is a low-cost and environmentally benign process, which has been used to synthesize various nanostructured materials, such as mesoporous nickel ferrites [24], hollow $BiFeO_3$ microspheres [25], and amorphous metal oxide catalysts [26]. In our previous studies, we adopted USP to fabricated a series of microsphere photocatalysts, including core-shell microspherical Ti_{1-x} Zr_xO_2 solid solutions [27], B-Ni-codoped TiO_2 solid and hollow microspheres [28], Bi_2WO_6 [29], and $PbWO_4$ [23]. Compared with other conventional methods for fabrication of porous structured catalysts, USP is a template-free method which can produce products with high purity. Most recently, Overcash and coworkers reported the fabrication of high surface area iron oxide microspheres of different morphologies, sizes, and crystallinities via USP method [30]. Wolframite $ZnWO_4$, however, has not been previously prepared with hierarchical porous structure through USP method.

In this study, wolframite $ZnWO_4$ with porous structures were prepared using the continuous, scalable process of ultrasonic spray pyrolysis at different preparation temperature for the first time, and the photocatalytic performance of the material were evaluated by gaseous NO_x degradation under simulated solar light irradiation. The physical and chemical properties of the resulting products were fully characterized and the photocatalytic degradation mechanism of NO_x over the as-prepared porous $ZnWO_4$ was elucidated in detail.

2. Experimental

2.1. Synthesis of hierarchical porous $ZnWO_4$

Zinc (II) nitrate hexahydrate ($Zn(NO_3)_2{\cdot}6H_2O$), tungstic acid (H_2WO_4), and ammonia were obtained from Sinopharm Chemical Reagent Co., Ltd. (Shanghai, China). All chemicals used for synthesis were of analytical grade and used without further purification. Deionized water was provided by Millipore® Milli-Q water purification system (Merck Millipore, Darmstadt, Germany). Hierarchical $ZnWO_4$ samples with porous structures were synthesized through ultrasonic spray pyrolysis (USP) method. For the preparation of $ZnWO_4$ microspheres, 10 mmol of zinc nitrate ($Zn(NO_3)_2$) and 10 mmol of tungstic acid were first dissolved in 10 mL of deionized water and 10 mL of concentrated ammonia solution, respectively. Subsequently, the tungstic acid/ammonia solution was added into the $Zn(NO_3)_2$ aqueous solution and stirred for about half an hour. Finally, the mixed solution was diluted to 100 mL with deionized water. The aqueous solution was nebulized using an ultrasonic nebulizer at 1.7 MHz ± 10% (YUYUE 402AI, Shanghai, China). Aerosol droplets generated were carried through a tube furnace at 700 °C (OTF-1200X, Hefei, China) by an air flow. $ZnWO_4$ microspheres were also prepared at 650 °C and 750 °C under other identical conditions with the sample at 700 °C. The $ZnWO_4$ products were collected by percolators at the end of the tube furnace. The obtained products were washed with ethanol and deionized water several times, and then dried at 70 °C in air. The resulting $ZnWO_4$ product obtained from USP at finance temperature of 650 °C, 700 °C, and 750 °C was denoted as ZWO-650, ZWO-700, and ZWO-750, respectively.

2.2. Characterization

The crystalline structure of the as-prepared $ZnWO_4$ samples was characterized through X-ray powder diffraction (XRD; PANanalytical, X'pert, Almelo, the Netherlands) using a Cu Kα radiation source (λ = 1.5406 Å) at a scanning rate of 0.04° 2θ/s in the 2θ range of 10°–80°. The morphology of the samples was investigated through field-emission scanning electron microscopy (FE-SEM; JEOL Model JSM-6700F, Tokyo, Japan). The transmission electron microscopy study (TEM; JEOL Model JEM-2100HR) was performed on a JEOL JEM-2100HR electron microscopy instrument. The samples for TEM were prepared by dispersing the $ZnWO_4$ powders in ethanol, followed by dropping onto carbon-coated copper grids. A Varian Cary 100 Scan UV–vis system equipped with a labsphere diffuse reflectance accessory was used to obtain the reflectance spectra of the catalysts over a range of 200–800 nm. Labsphere USRS-99-010 was employed as a reflectance standard. The spectra were converted from reflection to absorbance by the Kubelka–Munk method. Photoluminescence (PL; F-7000, Hitachi, Japan) was used to investigate the optical properties of the as-prepared samples. The Brunauer–Emmett–Teller (BET) surface area and pore structure of $ZnWO_4$ samples were obtained from N_2 adsorption/desorption isotherms at 77 K by using an ASAP 2020 automatic analyzer (Micromeritics Instrument Corp., Norcross, GA, USA). The samples for electron spin-resonance spectroscopy (ESR; ER200-SRC, Bruker, Germany) were prepared by mixing 0.05 g of the as-prepared photocatalyst in a 25 mM 5,5′-dimethyl-1-pirroline-N-oxide (DMPO) solution with a 50 mL aqueous dispersion for DMPO–•OH or a 50 mL methanol dispersion for DMPO–$^{\bullet}O_2^-$, respectively, under irradiation with 254 nm ultraviolet (UV) light. After the photocatalytic activity test was completed, the intermediate and final products (nitrate and nitrite ions) remaining on the catalyst powders were extracted by immersing the powders into deionized water (6 mL) and measured with a Dionex-600 Ion Chromatograph (Dionex Inc., Sunny-vale, CA, USA) equipped with an IonPac AS14A column. The mobile phase was composed of a mixture of 1.8 mM Na_2CO_3 and 1.7 mM $NaHCO_3$ at a flow rate of 1.20 mL min^{-1}, and the injected sample volume was 20 μL. The detection limit for NO_2^- and NO_3^- is 15 mg L^{-1}.

2.3. Photocatalytic activity test

The photocatalytic activity of $ZnWO_4$ microspheres was investigated by degradation of NO at ppb levels in a continuous flow reactor at ambient temperature under simulated solar-light irradiation. The reaction chamber was made of a rectangular stainless steel vessel (30 cm L × 15 cm W × 10 cm H) and covered with a quartz window. The simulated solar-light, which supplied by a 300 W Xenon lamp with the wavelength range from 200 to 1100 nm (Perfect Light MICROSOLAR 300, Beijing, China) and the spectral composition of the light source is shown in Fig. S1. The light beam vertically passed through the quartz window. For each photocatalytic activity test experiment, one sample dish (with a diameter of 12 cm) containing the photocatalyst powders was placed in the

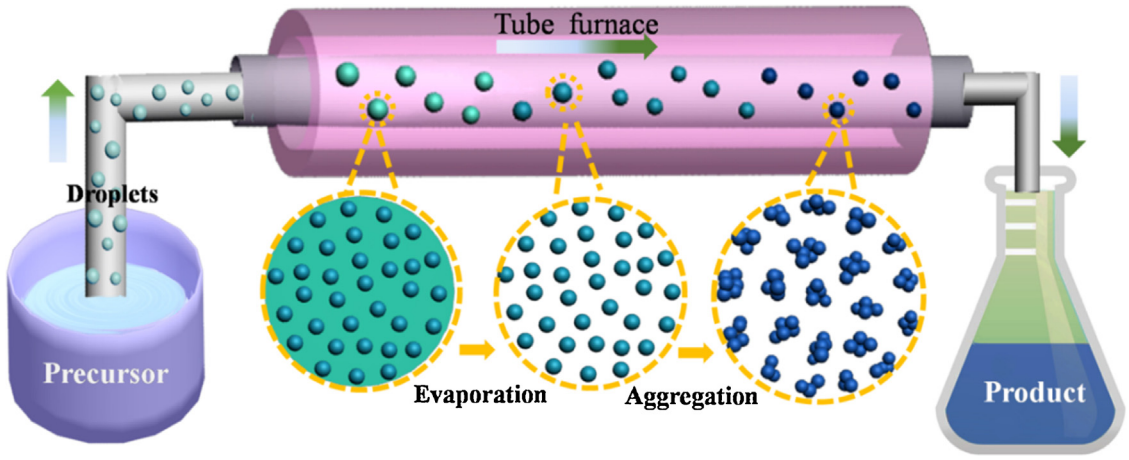

Scheme 1. Schematic diagram of porous $ZnWO_4$ microspheres formation through ultrasonic spray pyrolysis.

center of the reactor. The photocatalyst samples were prepared by coating an aqueous suspension of $ZnWO_4$ product onto a glass dish. The weight of the photocatalysts used for each experiment was kept at 0.1 g. The dishes containing the photocatalyst were pretreated at 70 °C for several hours until complete removal of water in the suspension and then cooled to room temperature before the photocatalytic test.

The NO gas was acquired from a compressed gas cylinder with the initial concentration of 50 ppm. The initial NO concentration for photocatalytic test was diluted to 400 ppb by the air stream supplied by a zero-air generator (Model 1001, Sabio Instruments LLC, Georgetown, TX, USA). The desired humidity level of the NO flow was controlled at 70% by passing the zero air streams through a humidification chamber. The gas streams were premixed completely by a gas blender and the flow rate was controlled at 3 L min^{-1} by a mass flow controller. After catalyst achieving adsorption/desorption equilibrium, the Xenon lamp was switched on. The concentrations of NO and NO_2 were continuously measured by a chemiluminescence NO_x analyzer (Model 42c, Thermo Environmental Instruments Inc., Franklin, MA, USA) during the photocatalytic degradation process, with a sampling rate of 0.7 L min^{-1}. The reaction of NO with air was ignorable when performing a control experiment with or without light in the absence of the photocatalyst. The NO removal rate was calculated by the following equation

$$D = (C_0 - C)/C_0 \times 100\%$$

Where D is the NO removal rate, C_0 represents the initial concentration of NO (ppb), and C is the NO concentration (ppb) measured in real time.

3. Results and discussion

3.1. Phase structure and morphology

Fig. 1 shows the XRD patterns of the as-prepared $ZnWO_4$ products synthesized by ultrasonic spray pyrolysis method at different temperature. The diffraction peaks in all the three samples can be readily indexed to monoclinic wolframite $ZnWO_4$ with a unit cell of a = 4.691 Å, b = 5.720 Å, and c = 4.925 Å (JCPDS card No.15-774, space group of P2/*c*). The strong and sharp peaks at (1 1 1), (1 0 0), and (0 2 1) planes suggest that the prepared $ZnWO_4$ samples are highly crystalline. Using Scherrer Equation, the average particle sizes of different samples were calculated using (1 1 1) diffraction peak and presented in Table 1. $D = 0.9\lambda/(B \cos \theta)$,where 0.9 is the typical value for the shape factor K, λ is the X-ray wavelength, B is the line broadening full width at half maximum (FWHM) of peak height in radians, and θ is the Bragg diffraction angle. As observed, with the rise of pyrolysis temperature, the crystallite size slightly increases from 12.9 nm to 13.6 nm accordingly (as shown in Table 1), suggesting the crystal growth along with the temperature rise. Moreover, during the synthesis processes, the synthesis temperature shows dramatic influences on the phase structure of $ZnWO_4$ samples. As shown in Fig. S2, as the temperature <650 °C or >750 °C, no pure phase of $ZnWO_4$ was obtained, indicating that the pyrolysis temperature critically influences the crystallinity of $ZnWO_4$ during the USP synthesis processes.

Fig. 2a–c shows the typical SEM images of the as-prepared $ZnWO_4$ microspheres from ultrasonic spray pyrolysis at 650, 700 and 750 °C, respectively. It is clearly seen that the resulting $ZnWO_4$ samples were composed of hierarchical microspheres with diameter ranging from 0.1 to 2 μm. As depicted in Fig. 2a–c, the surfaces of the microspheres are not smooth, suggesting that the resulting microspheres are formed by the aggregation of nanoparticles, which is also observed in our previous studies [29]. Moreover, it is noted that few smooth spheres and spheres with irregular structures were present in the ZWO-650 and ZWO-750 batches, respectively. This finding suggests that temperature affects the surface texture of the $ZnWO_4$ produced. The close-up view of ZWO-700 (Fig. 2d) indicates that the as prepared $ZnWO_4$ possess pores and cavities on the surface of the spheres. This morphology was probably the result of rapid solvent evaporation at high pyrolyzing temperatures and subsequent shell cracking [30].

The spherical and porous structures of the as-prepared ZWO-700 sample were further confirmed by TEM, as shown in Fig. 3. Fig. 3a demonstrates that the ZWO-700 is porous structured microspheres and built by the aggregation of a large quantity of nanoparticles with a crystallite size of 15 nm. Additionally, Fig. S3 also further exhibited that the $ZnWO_4$ microspheres were

Table 1
Brunauer–Emmett–Teller (BET) surface area, pore volume, pore size, and crystallite size of the sample batches.

Sample batch	S_{BET} (m^2/g)[a]	V_p (cm^3/g)[b]	Pore size (nm)[c]	Crystallite size (nm)[d]
ZWO-650	9.71	0.05	22.2	12.9
ZWO-700	15.48	0.09	24.7	13.2
ZWO-750	10.03	0.05	21.6	13.6

[a] BET surface area calculated from the linear part of the BET plot.
[b] Pore volume obtained from the volume of N_2 adsorbed.
[c] Average pore diameter estimated using the adsorption branch of the isotherm and the Barrett–Joyner–Halenda formula.
[d] Average crystallite size calculated using the Scherrer Equation.

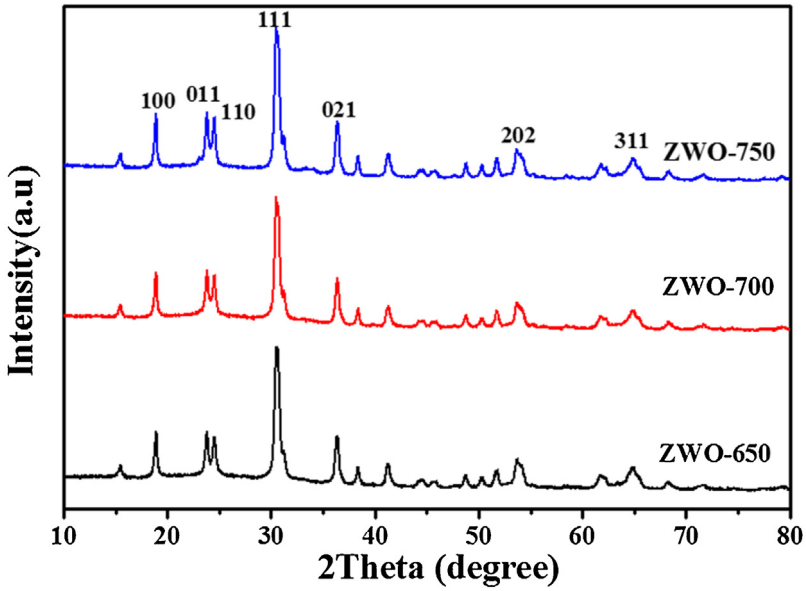

Fig. 1. XRD patterns of the as-prepared ZWO-650, ZWO-700, and ZWO-750 samples.

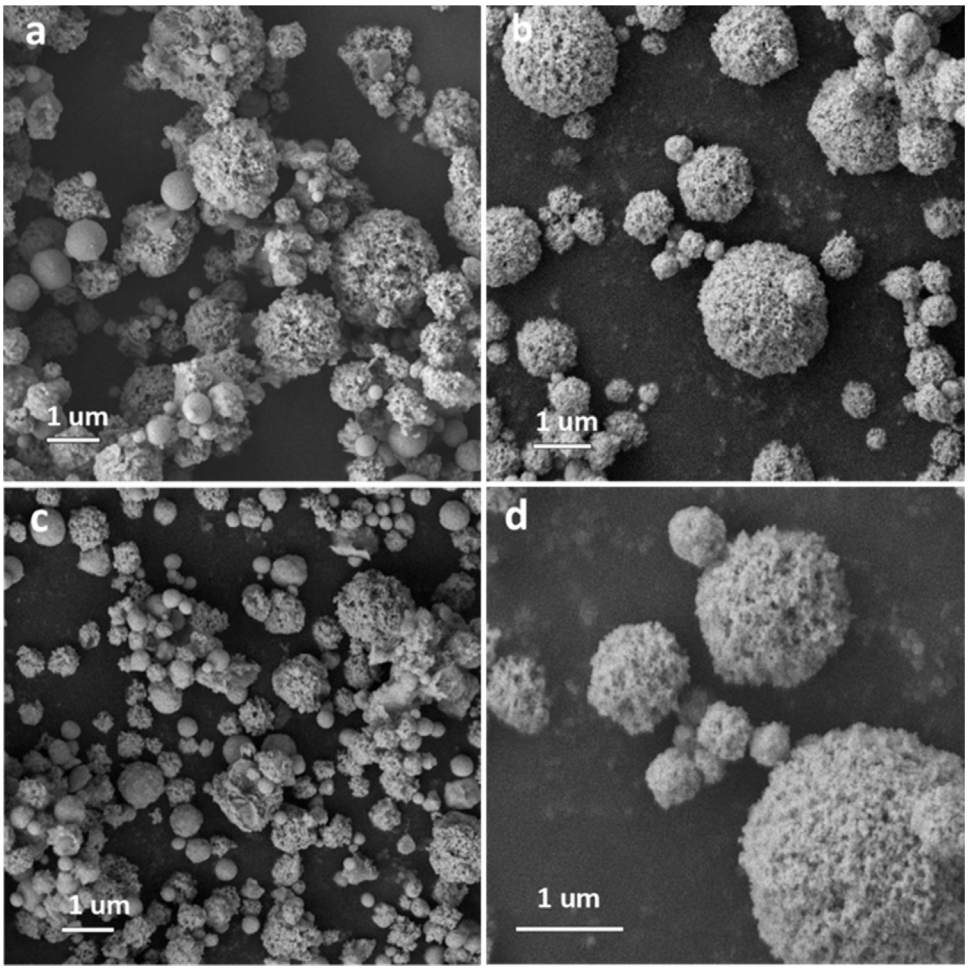

Fig. 2. SEM images of $ZnWO_4$ microspheres prepared through USP: (a) ZWO-650, (b) ZWO-700, (c) ZWO-750, and (d) a magnified image of ZWO-700 microspheres.

composed of a large number of nanospheres. This observation is consistent with the crystallite size calculated from XRD patterns as shown in Table 1. The aggregation and/or self-assembly of the nanoparticles can produce abundant hierarchical pores at nanoscale. High-resolution TEM (HRTEM) image (Fig. 3b) was recorded at the edge of an individual $ZnWO_4$ sphere. It indicates that the single-crystalline nature of the nanoparticles and clarifies the particular orientation of the nanoparticles. The *d*-spacing

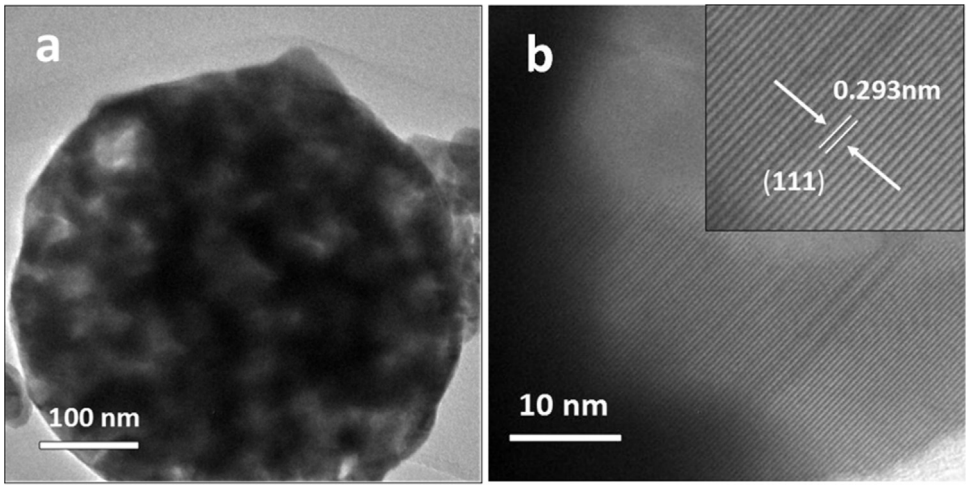

Fig. 3. TEM images of ZWO-700 microspheres: (a) low-magnification, and (b) high-resolution TEM images of $ZnWO_4$ microspheres obtained from the edge of the microspheres.

is 0.293 nm, which agrees well with the lattice spacing of (1 1 1) of the monoclinic $ZnWO_4$.

3.2. Surface area and pore structures

The N_2 adsorption-desorption isotherms and pore size distribution curves of samples ZWO-650, ZWO-700, and ZWO-750 are shown in Fig. S4. The pore size distribution was calculated from desorption branch of nitrogen isotherms by Barret-Joyner-Halenda (BJH) method using the Halsey equation. The physioadsorption isotherms as shown in Fig. S4a can be classified as type IV with hysteresis loops according to the IUPAC classification, suggesting the presence of porous structure in the as-prepared $ZnWO_4$ samples [31]. The pore diameters were mainly distributed within the range of 5–30 nm, and the average pore size is around 20 nm (Table 1). The specific surface area, average pore size, and pore volume of the samples are summarized in Table 1. The ZWO-700 sample processed the highest BET surface area (15.48 m^2/g) than those of ZWO-650 (9.71 m^2/g) and ZWO-750 (10.03 m^2/g), which is also true for the pore volume. The high surface area can probably facilitate the mass transfer of air pollutants or reaction intermediates during the photocatalytic reaction processes. Therefore, it is expected that the high surface area and high crystallinity of our products could enhance the photocatalytic activity.

A possible formation mechanism for porous $ZnWO_4$ microspheres produced through USP is illustrated in Scheme 1. Based on the experimental results and observations, we propose that the formation process consists of the following three sequential stages: (1) the precursor droplets containing $Zn(NO_3)_2$ and $(NH_4)_2WO_4$ was generated by the ultrasonic nebulizer; (2) the produced droplets pass through the tubular furnace, where the high temperature induces the solvent evaporation and the formation of $ZnWO_4$ nanoparticles; and (3) the further annealing results in the self-assembly and aggregation of $ZnWO_4$ nanoparticles, leading to the formation of porous microspheres. This is consistent with the SEM results as shown in Fig. 2 which shows that the droplets tended to cluster with continuous heating and finally self-assembled into microspheres with diameters of 0.1 to 2 μm. The rapid evaporation of solvents during the pyrolysis processes promoted the formation of porous structures.

3.3. Optical properties

Fig. 4 shows the UV–vis absorption spectra of sample ZWO-650, ZWO-700, and ZWO-750, respectively. The results show that all samples present excellent photoabsorption at wavelengths shorter than 420 nm. Moreover, the absorption curve of sample ZWO-700 shows significant red shift as compared with those of ZWO-650 and ZWO-750. Assuming $ZnWO_4$ acted as a direct-band gap semiconductor, the band gap energies (E_g) were estimated by extrapolation of the linear part of the $(ah\upsilon)^2$ versus $h\upsilon$ plots (where α is the absorption coefficient, and hυ is the photon energy) [32]. As a result, the E_g values of ZWO-650, ZWO-700, and ZWO-750 were explored as 3.46, 3.37, and 3.72 eV, respectively (inset of Fig. 4). Our synthesized $ZnWO_4$ shows slightly higher E_g values than that reported by Kim and coworkers, of which the value is 2.95 eV [33]. This difference may be due to the different crystal structural environments, such as the W—O bond lengths. As reported by kim et al. [33], $ZnWO_4$, as the typical wolframite structure, the tungsten atom is surrounded by six oxygen atoms to form WO_6 octahedra, and its conduction band and valence band were mainly consisted of the W 5d orbitals and O 2p orbitals. Thus the different interactions between the orbitals of W and O elements in different crystal field would influence the band gap. Other studies also indicated that the electronic band structures are strongly influenced by the crystal structure [34–36]. A shorter band length induces the stronger interaction between metal and oxygen orbital and leads to a higher band gap. Therefore, we speculate that the different band-gap values of our $ZnWO_4$ microspheres can be attributed to the variations in the microsphere structures.

3.4. Photocatalytic performance on NO degradation

The photocatalytic efficiency of the as-prepared $ZnWO_4$ samples was evaluated by the degradation of NO under simulated solar-light irradiation in a continuous reactor. Fig. 5a shows the variation of NO concentration (C/C_0) with irradiation time over the obtained $ZnWO_4$ microspheres. Here, C_0 is the initial concentration of NO, and C is the concentration of NO after photocatalytic degradation for time *t*. As a comparison, photocatalytic oxidation of NO over commercial P25 was also performed under identical conditions. As shown in Fig. 5a, the NO concentration drastically decreased after the simulated solar light was turned on, and it reached the steady state after about 10 min. The sample ZWO-700 shows the highest photocatalytic activity and the NO removal ratio reached about 40%, which is much higher than that of commercial P25. The NO removal ratios over ZWO-650 and ZWO-750 are 29% and 25%, respectively. This observation indicates that the pyrolysis temperature of USP significantly affect the photocatalytic activity of $ZnWO_4$ because of the influence on the microstructures of photocatalyst.

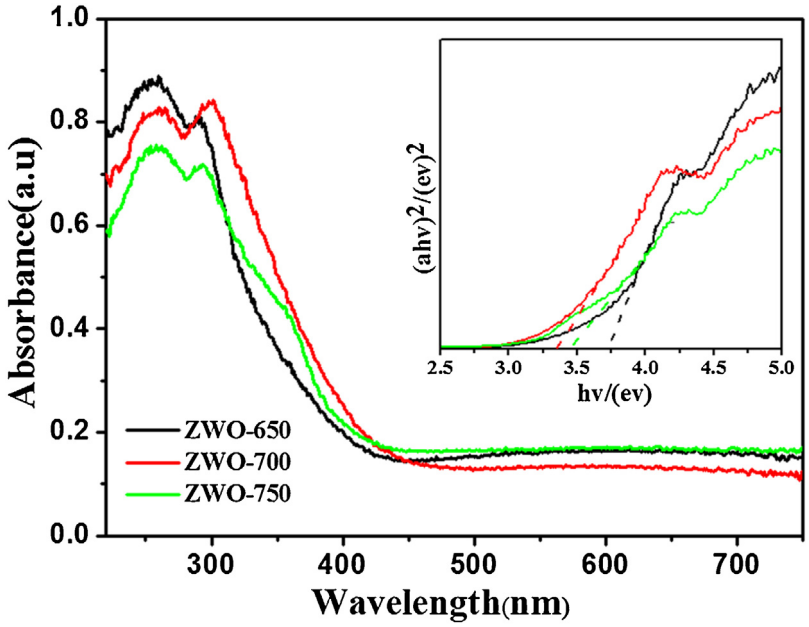

Fig. 4. UV–vis absorption spectra of the as-prepared ZWO-650, ZWO-700, and ZWO-750 batch samples. The inset shows the T_c plot of $(\alpha h\nu)^2$ versus photon energy ($h\nu$) for different samples.

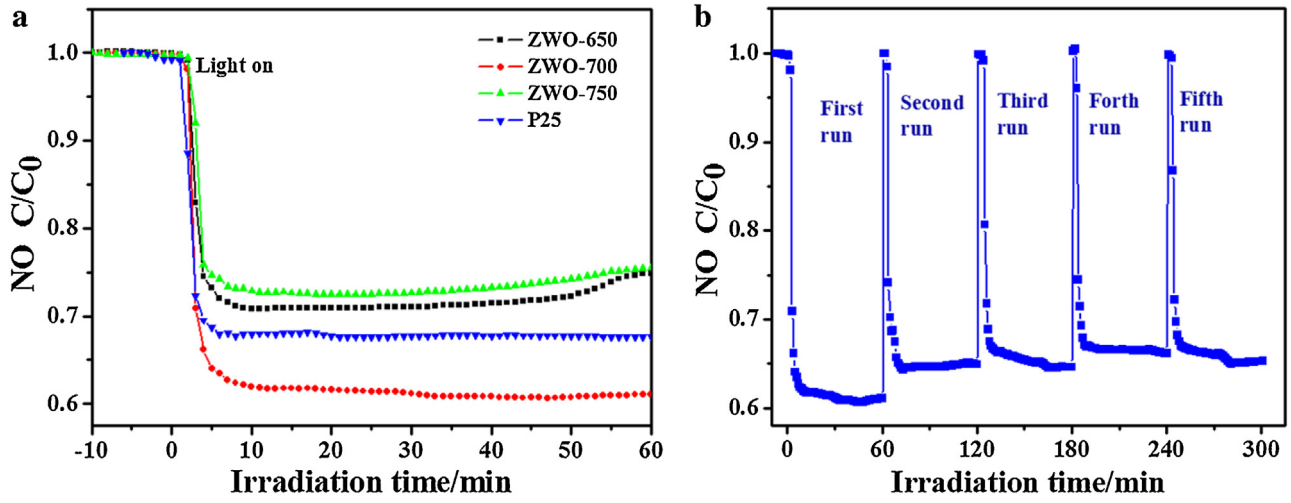

Fig. 5. (a) NO photocatalytic degradation under solar light irradiation for different $ZnWO_4$ microsphere batches and (b) photochemical stability of the ZWO-700 sample.

Moreover, it was found that the NO removal efficiencies over ZWO-650 and ZWO-750 decreased about 5% after 60 min reaction, which can be ascribed to the accumulation of nitrate on the photocatalyst surface [37–39]. Interestingly, the photocatalytic activity of NO removal over ZWO-700 did not show any deactivation, which might be attributed to its porous structure with a high surface area and smaller particle size, and eventually facilitated the diffusion of NO and reaction products.

To further study the stability of the porous ZWO-700 microspheres on photocatalytic oxidation of NO in gas phase, we carried out the multiple runs of photocatalytic experiment with the used ZWO-700 microspheres. As shown in Fig. 5b, the highest NO removal efficiencies reached 40% during the degradation of first run, and hardly any decrease later. When entered the second loop, the NO degradation ratio is slight reduce, which may be due to the special porous structure. $ZnWO_4$ microspheres could adsorb more NO into the internal pore canal in the first run. It was interesting to find the catalyst only exhibited negligible deactivation after next four cycles of repeated experiments, and the removal efficiency is still not less than 35%, suggesting that the $ZnWO_4$ microspheres is relatively stable and is not easy to photo-corroded during the photocatalytic degradation.

3.5. Insights into the photocatalytic degradation mechanism of NO

The separation of electron and hole pairs after light irradiation is the fundamental process for semiconductor photocatalysis. The electron and hole pairs could migrate to the semiconductor surfaces and be captured by the surface adsorbed O_2 and H_2O to produce $^{\bullet}O_2^-$ and $^{\bullet}OH$ radicals, respectively. These generated radicals can eventually lead to the efficient destruction of air pollutants. In order to fully understand the photocatalytic mechanism for the as-prepared porous $ZnWO_4$ microspheres, electron spin resonance spectroscopy (ESR) method was adopted for the direct identification and quantification of short-lived $^{\bullet}OH$ and $^{\bullet}O_2$- radicals

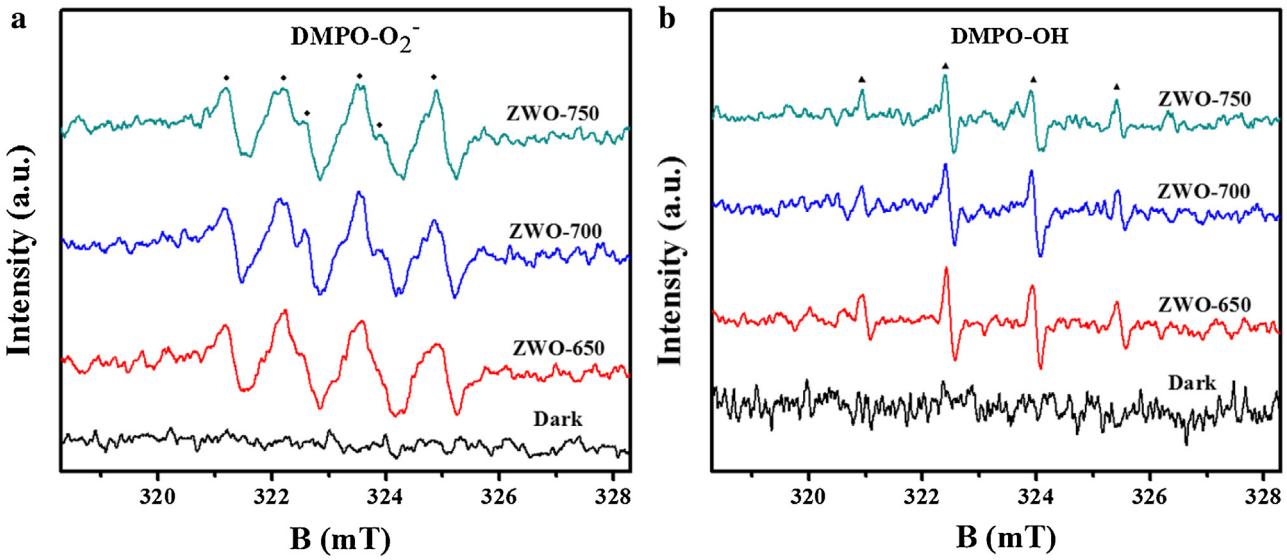

Fig. 6. Electron spin resonance (ESR) spectra of radical adducts trapped for different $ZnWO_4$ samples by (a) DMPO-$^{\bullet}O_2^-$ and (b) DMPO-$^{\bullet}$OH with or without 10 min illumination of ultraviolet light.

during the photodegradation of NO over as-prepared $ZnWO_4$ photocatalysts, with DMPO as the spin-trap reagent under simulated solar-light irradiation [40,41]. As shown in Fig. 6a and b, the characteristic ESR signals of $^{\bullet}$OH and $^{\bullet}O_2^-$ radicals were absent without UV light irradiation. Upon irradiation for 10 min in the presence of $ZnWO_4$ samples synthesized at different temperature, we clearly observed a six-line spectrum with the hyperfine splitting parameter of $a^N = 1.36$ mT, $a^{\beta}H = 1.07$ mT, suggesting the formation of the adduct between DMPO and superoxide, DMPO-$O_2^{\bullet-}$ (Fig. 6a) [42–44]. Meanwhile, a four-line spectrum with an intensity ratio of 1:2:2:1 (Fig. 6b) were also observed after 10 min of UV light irradiation with the existence of as-prepared $ZnWO_4$ samples, and the hyperfine splitting parameter is $a^N = a^H = 1.49$ mT, suggesting the formation of DMPO-$^{\bullet}$OH[45]. Therefore, the ESR spectra confirms the formation of $^{\bullet}$OH and $^{\bullet}O_2^-$ radicals during the photocatalysis processes, and both of them play a crucial role in photodecomposition of NO. Based on the above results, both $^{\bullet}$OH and $^{\bullet}O_2^-$ radicals were involved in the photocatalytic reaction associated with $ZnWO_4$ samples, which is consistent with theoretical estimation by comparing the band edge energies of $ZnWO_4$ with the redox potentials of relevant species. As reported by Kim et al. [33], the conduction band potential (E_c) of $ZnWO_4$ was about −0.799 eV which is more negative than E^0 ($O_2/^{\bullet}O_2^-$, −0.33 eV), while the valence band potential (E_c) is 2.15 eV which is more positive than E^0 ($OH^-/^{\bullet}$OH, +1.99 eV). These analysis demonstrated that the production of $^{\bullet}$OH and $^{\bullet}O_2^-$ radicals during the photocatalysis processes over the as-prepared $ZnWO_4$ samples is thermodynamically favorable.

Moreover, it is interesting to find that the signal intensities of $^{\bullet}$OH and $^{\bullet}O_2^-$ radicals over ZWO-700 sample are the highest among ZWO-650, ZWO-700 and ZWO-750. This was probably due to the improved charge separation efficiency over sample ZWO-700 because of its superior porous structure, particle size and crystallinity. Generally, the activities of photocatalysts are mainly determined by the optical absorption capability, specific surface area, and separation/diffusion rate of the photogenerated charge carriers. As shown in Fig. 5a, ZWO-700 shows the highest NO removal ratio among all the three $ZnWO_4$ samples obtained from USP method. Based on the characterization results, this higher photocatalytic activity of the ZWO-700 sample is probably attributed to the following two aspects: (1) suitable particle size and crystallinity. It is well-accepted that small particle size may provide high surface area and more active sites, while crystallinity determines the separation rates of photogenerated charge carriers. When the pyrolysis temperature varied from 650 °C to 750 °C, the crystallite size of sample ZWO-650, ZWO-700, and ZWO-750 were 12.9 nm, 13.2 nm and 13.6 nm, respectively. The ZWO-700 sample also shows the highest BET surface area, which is beneficial for the enhancement of photocatalytic activities. However, the small particle size of ZWO-650 led to poor crystallinity and therefore reduced photocatalytic performances, (2) enhanced light absorption ability and porous structure. A smaller band gap is effective in generating charge carriers. Moreover, charge carrier mobility is an important indicator of transferring the photogenerated charge carriers from bulk to the surface. As shown in Fig. 4, the E_g value of ZWO-700 is the smallest among all the three samples, suggesting its superior light absorption ability. The photoluminescence (PL, Fig. 7) emission is a useful technique for investigating the generation, transfer, and recombination of photogenerated charge carriers. A low intensity of PL spectra indicates a high separation efficiency of electron-hole pairs. The PL spectra of ZWO-650, ZWO-700 and ZWO-750 were recorded with the excitation wavelength at 300 nm. All $ZnWO_4$ samples present broad emission peaks from 300 to 600 nm, and the peaks centered at 463 nm which is consistent with the previous studies [28]. The photoluminescent properties of $ZnWO_4$ are attributed to the charge-transfer transition between the empty d orbitals of the central W and the O 2p orbitals in the W (d°)-O (-II) groups [46]. The peak intensity varied significantly suggesting the synthesis temperature has a significant impact on the catalyst structures. Consistent with the results of activity, the as-prepared ZWO-700 samples exhibit the lowest PL intensity, indicating that the charge-carrier recombination rate is relatively slow.

Therefore, based on the characterization results and analysis of our synthesized porous structured $ZnWO_4$ microspheres, we propose a possible photocatalytic reaction mechanism for NO removal over $ZnWO_4$ microspheres under simulated solar light irradiation, as shown in Fig. 8. As a consequence, the poisonous gas could be oxidized to nitrate via active radicals with strong redox ability. The accumulated amount of nitrate (NO_3^-) and nitrite ions (NO_2^-) on the surfaces of $ZnWO_4$ samples after the photoactivity test were determined by ion chromatography method, and the results are presented in Table S1. It was found that the amount of NO_3^- accumulated on ZWO-650, ZWO-700, and ZWO-750 surfaces were 57.10 ug/m^2, 38.93 ug/m^2, and 46.22 ug/m^2, respectively. It suggested that the high specific surface area of ZWO-700 facilitated

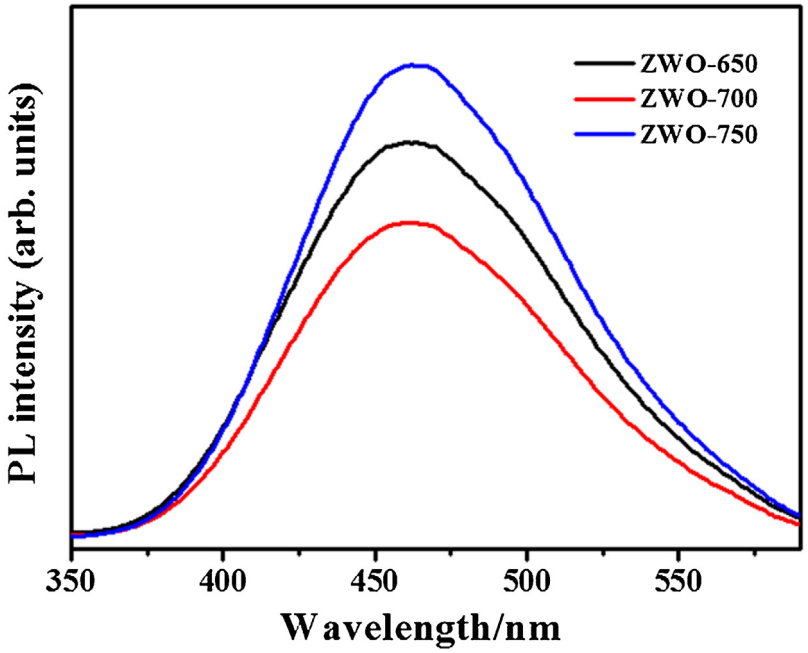

Fig. 7. Photoluminescence (PL) spectra of ZWO-650, ZWO-700, and ZWO-750 microsphere samples.

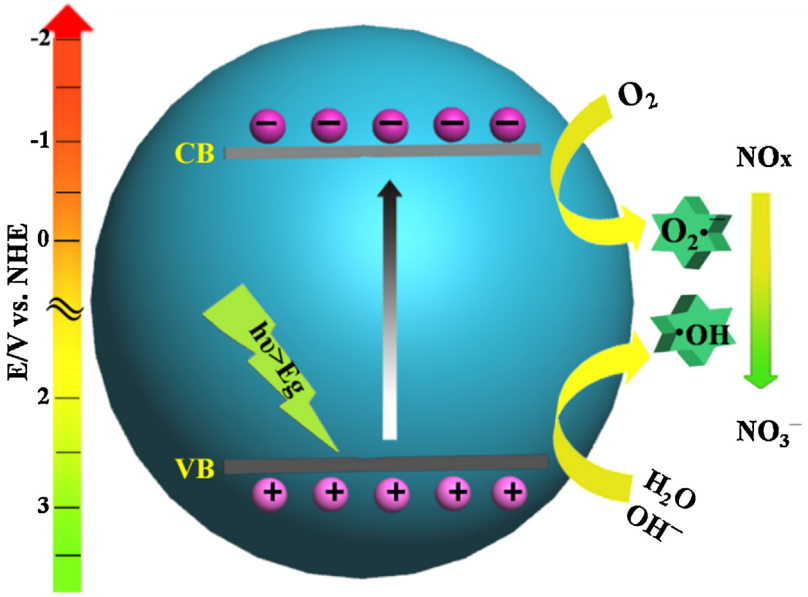

Fig. 8. Schematic diagram of the photocatalytic degradation mechanism of NO with the as-prepared $ZnWO_4$ microspheres under simulated solar-light irradiation.

the diffusion of reaction products which is beneficial for the enhancement of photocatalytic activity. Moreover, NO_2^- is an unstable intermediate, and it showed only a weak signal in the samples, probably because this active species has a strong redox potential and is capable of oxidizing the majority of the NO into NO_3^-. These results provide an accurate estimation of the final products from NO degradation by $ZnWO_4$ microspheres. Ai et al. [37] have also reported that NO_3^- is the major product formed after the photocatalytic oxidation of gaseous NO, but a small amount of NO_2^- also can be generated. Thus, the reaction pathway for NO removal over $ZnWO_4$ includes the following steps:

$$ZnWO_4 + h\upsilon \rightarrow ZnWO_4(e^-) + ZnWO_4(h^+)$$

$$e^- + O_2 \rightarrow {}^\bullet O_2^-$$

$${}^\bullet O_2^- + H^+ \rightarrow HO_2^\bullet$$

$$2HO_2^\bullet \rightarrow H_2O_2 + O_2$$

$$H_2O_2 + e^- \rightarrow {}^\bullet OH + OH^-$$

$$OH^- + h^+ \rightarrow {}^\bullet OH$$

$$NO + {}^\bullet O_2^- \rightarrow NO_3^-$$

$$2\,{}^\bullet OH + NO \rightarrow NO_2 + H_2O$$

$$NO_2 + {}^\bullet OH \rightarrow NO_3^- + H^+$$

Firstly, the electrons of $ZnWO_4$ are excited from the valence band to the conduction band upon simulated solar light irradiation. The holes left in VB could react with hydroxyl groups/water to form hydroxyl free radicals because of its suitable electrode potential position, thereby leading to the effective separation of photo-generated carriers. Moreover, the electrons in CB were able to reduce oxygen to $^{\bullet}O_2^-$ because of its much more negative electrode potential position. The as-prepared $ZnWO_4$ samples showed specific porous structures, which allowed the rapid transfer of photo-generated electrons to the surface where they can participate in photocatalytic reactions: this is why the pore structure of the catalyst is an important factor influencing NO degradation.

4. Conclusions

Hierarchical porous $ZnWO_4$ microspheres were successfully synthesized through ultrasonic spray pyrolysis method. The photocatalyitc removal of NO under simulated solar light irradiation and associated degradation mechanisms over these resultants were further investigated. It was found that synthesis temperature was a key factor influencing the microstructures of resulting $ZnWO_4$ samples which eventually affect their photocatalytic activity. The sample ZWO-700 exhibited superior activity than those of ZWO-650 and ZWO-750, which could be explained by its improved optical absorption capability, high specific surface area, and fast separation/diffusion rate of the photogenerated charge carriers. ESR analysis indicated that $^{\bullet}O_2^-$ and $^{\bullet}OH$ radicals function as active species for NO degradation. This study shows that porous structured $ZnWO_4$ microspheres with high activity can be readily prepared by ultrasonic spray pyrolysis method which is a promising approach for large scale production.

Conflict of interest

The authors declare no competing financial interest.

Acknowledgments

This research was financially supported by the National Science Foundation of China (41401567, 41573138), and was also partially supported by Research Grants Council of Hong Kong (PolyU 152083/14E), the research grant of Early Career Scheme (ECS 809813) from the Research Grant Council, Hong Kong SAR Government. Yu Huang is also supported by the "Hundred Talent Program" of the Chinese Academy of Sciences.

Appendix A. Supplementary data

Supplementary data associated with this article can be found, in the online version, at http://dx.doi.org/10.1016/j.apcata.2016.02.007.

Spectral composition of the light source, XRD patterns of the as-prepared ZWO-600 and ZWO-800 samples, N_2 adsorption/desorption isotherms and pore size distribution, concentration of nitrate ions from $ZnWO_4$ samples after photo-degradation reaction. The Supporting information is available free of charge on the publication website.

References

[1] R.J. Huang, Y.L. Zhang, C. Bozzetti, K.F. Ho, J.J. Cao, Y.M. Han, K.R. Daellenbach, J.G. Slowik, S.M. Platt, F. Canonaco, P. Zotter, R. Wolf, S.M. Pieber, E.A. Bruns, M. Crippa, G. Ciarelli, A. Piazzalunga, M. Schwikowski, G. Abbaszade, J. Schnelle-Kreis, R. Zimmermann, Z.S. An, S. Szidat, U. Baltensperger, I. El Haddad, A.S.H. Prevot, Nature 514 (2014) 218–222.
[2] I. Heo, M.K. Kim, S. Sung, I.S. Nam, B.K. Cho, K.L. Olson, W. Li, Environ. Sci. Technol. 47 (2013) 3657–3664.
[3] S. Roy, M.S. Hegde, G. Madras, Appl. Energy 86 (2009) 2283–2297.
[4] P. Granger, V.I. Parvulescu, Chem. Rev. 111 (2011) 3155–3207.
[5] J.R. Kastner, K.C. Das, J. Air Waste Manage. 52 (2002) 459–469.
[6] J.R. Kastner, K.C. Das, J. Chem. Technol. Biot. 80 (2005) 1170–1179.
[7] Q.B. Guo, T.H. Sun, Y.L. Wang, Y. He, J.P. Jia, Environ. Sci. Technol. 47 (2013) 9514–9522.
[8] W.S. Epling, L.E. Campbell, A. Yezerets, N.W. Currier, J.E. Parks, Catal. Rev. 46 (2004) 163–245.
[9] R. Shi, Y. Wang, D. Li, J. Xu, Y. Zhu, Appl. Catal. B Environ. 100 (2010) 173–178.
[10] J. Lin, J. Lin, Y.F. Zhu, Inorg. Chem. 46 (2007) 8372–8378.
[11] H.B. Fu, J. Lin, L.W. Zhang, Y.F. Zhu, Appl. Catal. A Gen. 306 (2006) 58–67.
[12] R. Dafinova, K. Papazova, A. Bojinova, J. Mater. Sci. Lett. 17 (1998) 237–239.
[13] A. Golubovic, R. Gajic, Z. Dohcevic-Mitrovic, S. Nikolic, J. Alloy. Compd. 415 (2006) 16–22.
[14] D. Li, R. Shi, C.S. Pan, Y.F. Zhu, H.J. Zhao, CrystEngComm 13 (2011) 4695–4700.
[15] J. Yu, J.C. Yu, W. Ho, M.K.P. Leung, B. Cheng, G. Zhang, X. Zhao, Appl. Catal. A Gen. 255 (2003) 309–320.
[16] Z. Amouzegar, R. Naghizadeh, H.R. Rezaie, M. Ghahari, M. Aminzare, Ceram. Int. 41 (2015) 1743–1747.
[17] R. Shi, Y.J. Wang, D. Li, J. Xu, Y.F. Zhu, Appl. Catal. B Environ. 100 (2010) 173–178.
[18] H.W. Shim, I.S. Cho, K.S. Hong, A.H. Lim, D.W. Kim, J. Phys. Chem. C 115 (2011) 16228–16233.
[19] G.Q. Tan, L.L. Zhang, S.S. Wei, A. Xia, H.J. Ren, Cryst. Res. Technol. 47 (2012) 1279–1283.
[20] M. Wang, Y.F. Tang, T.M. Sun, G.Q. Jiang, Y.J. Shi, CrystEngComm 16 (2014) 11035–11041.
[21] Y.X. Zhou, L. Tong, X.B. Chen, X.H. Zeng, Appl. Phys. A Mater. 117 (2014) 673–679.
[22] D. Li, R. Shi, C. Pan, Y. Zhu, H. Zhao, CrystEngComm 13 (2011) 4695–4700.
[23] F. Dong, Y. Huang, S.C. Zou, J.A. Liu, S.C. Lee, J. Phys. Chem. C 115 (2011) 241–247.
[24] D. Hong, Y. Yarnada, M. Sheehan, S. Shikano, C.H. Kuo, M. Tian, C.K. Tsung, S. Fukuzumi, ACS Sustainable Chem. Eng. 2 (2014) 2588–2594.
[25] Y.N. Huo, M. Miao, Y. Zhang, J.A. Zhu, H.X. Li, Chem. Commun. 47 (2011) 2089–2091.
[26] L. Kuai, J. Geng, C. Chen, E. Kan, Y. Liu, Q. Wang, B. Geng, Angew. Chem. Int. Ed. 53 (2014) 7547–7551.
[27] Y. Huang, Z. Zheng, Z.H. Ai, L.Z. Zhang, X.X. Fan, Z.G. Zou, J. Phys. Chem. B 110 (2006) 19323–19328.
[28] Y. Huang, W. Ho, Z. Ai, X. Song, L. Zhang, S. Lee, Appl. Catal. B Environ. 89 (2009) 398–405.
[29] Y. Huang, Z.H. Ai, W.K. Ho, M.J. Chen, S. Lee, J. Phys. Chem. C 114 (2010) 6342–6349.
[30] J.W. Overcash, K.S. Suslick, Chem. Mater. 27 (2015) 3564–3567.
[31] K.S.W. Sing, D.H. Everett, R.A.W. Haul, L. Moscou, R.A. Pierotti, J. Rouquerol, T. Siemieniewska, Pure Appl. Chem. 57 (1985) 603–619.
[32] J.W. Tang, Z.G. Zou, J.H. Ye, J. Phys. Chem. B 107 (2003) 14265–14269.
[33] D.W. Kim, I.S. Cho, S.S. Shin, S. Lee, T.H. Noh, D.H. Kim, H.S. Jung, K.S. Hong, J. Solid State Chem. 184 (2011) 2103–2107.
[34] I.S. Cho, C.H. Kwak, D.W. Kim, S. Lee, K.S. Hong, J. Phys. Chem. C 113 (2009) 10647–10653.
[35] S.X. Ouyang, N. Kikugawa, D. Chen, Z.G. Zou, J.H. Ye, J. Phys. Chem. C 113 (2009) 1560–1566.
[36] S.X. Ouyang, Z.S. Li, Z. Ouyang, T. Yu, J.H. Ye, Z.G. Zou, J. Phys. Chem. C 112 (2008) 3134–3141.
[37] Z. Ai, W. Ho, S. Lee, L. Zhang, Environ. Sci. Technol. 43 (2009) 4143–4150.
[38] Z. Ai, Y. Huang, S. Lee, L. Zhang, J. Alloy. Compd. 509 (2011) 2044–2049.
[39] Z. Ai, S. Lee, Y. Huang, W. Ho, L. Zhang, J. Hazard. Mater. 179 (2010) 141–150.
[40] W. He, Y.T. Zhou, W.G. Wamer, X. Hu, X. Wu, Z. Zheng, M.D. Boudreau, J.J. Yin, Biomaterials 34 (2013) 765–773.
[41] Z. Wang, W. Ma, C. Chen, H. Ji, J. Zhao, Chem. Eng. J. 170 (2011) 353–362.
[42] S. Chen, Y. Hu, S. Meng, X. Fu, Appl. Catal. B Environ. 150–151 (2014) 564–573.
[43] J.R. Harbour, M.L. Hair, J. Phys. Chem. 82 (1978) 1397–1399.
[44] T. Yan, R. Yuan, W. Li, J. You, Appl. Catal. A Gen. 478 (2014) 204–210.
[45] H.T. Zhao, J. Joseph, H. Zhang, H. Karoui, B. Kalyanaraman, Free Radical Biol. Med. 31 (2001) 599–606.
[46] H. Wang, F.D. Medina, D.D. Liu, Y.D. Zhous, J. Phys. Condens. Matter 6 (1994) 5373–5386.